FRACTURE PROPERTIES OF SURFACE MODIFICATION LAYERS VIA A MODIFIED BI-LAYER BEAM MODEL

H. T. Liu

School of Mechanics and Engineering Science
Henan, China

M. H. Zhao*

School of Mechanics and Engineering Science
Henan, China

Henan Key Engineering Laboratory for Anti-Fatigue Manufacturing Technology
School of Mechanical Engineering
Henan, China

J. W. Zhang*

School of Mechanics and Engineering Science
Henan, China

ABSTRACT

A modified bi-layer beam model is proposed to study the fracture-dominated scratch process of the brittle material with surface modification layer considering residual stress. The nonlinear analytical solution of the energy release rate is derived considering the graded distribution of the elastic modulus and residual stress. Finite element analysis is also conducted. Both analytical and numerical results show that the graded distribution of the material properties and residual stress plays an important role in the fracture process. Based on the inverse analysis, the proposed model could provide a convenient way to determine the energy release rate of materials possessing a surface modification layer.

Keywords: Bi-layer beam model, Surface modification layer, Scratch, Energy release rate.

1. INTRODUCTION

The fracture properties of materials possessing a surface modification layer have drawn much attention in both academics and industry [1, 2]. To test the fracture property of these materials, indentation and scratch test methods [3-5] have been proposed in addition to the traditional method. However, key problems remain unsolved relating to the measurement of the fracture properties of the surface modification layer. First, the thickness of the surface modification layer, ranging from 200 μm all the way down to 5 μm or less [6-8], is a scale to which the traditional methods for measuring fracture properties can hardly be extended. Second, the mechanical property of the surface layer varies with depth [9], which makes it almost impossible to obtain fracture property variations using the indentation test method. Third, residual stress is always generated accompanying the formation of the surface modification layer [10], which makes the problem more complicated. Among the existing methods, however, the scratch test method remains the most promising method to assess the fracture mechanical properties when considering all three of the difficulties listed above.

The traditional scratch test has been used to investigate the mechanisms of abrasion for quite a long time [11, 12], where investigators have focused mainly on the elastic-plastic deformation processes resulting from wear and damage. Ulm *et al*. [13, 14] proposed a theoretical model to determine fracture toughness, adopting the scratch method within a framework of linear elastic fracture mechanics. They applied the Airy stress function approach to determine the stress and displacement in the vicinity of a scratch-blade-material interface, which served as the input for the evaluation of the J-integral. Their studies introduced the scratch test method to the field of fracture mechanics, presenting a convenient method to test mechanical fracture properties. However, Lin and Zhou [15, 16] challenged many aspects of their interpretations. The main controversies were around

* Corresponding author (memhzhao@zzu.edu.cn, memhzhao@sina.com; zhangjianwei@zzu.edu.cn)

DOI : 10.1017/jmech.2018.36
Copyright © 2018 The Society of Theoretical and Applied Mechanics
https://doi.org/10.1017/jmech.2018.36 Published online by Cambridge University Press

the following three points. (1) Whether the direction of the crack is along the direction of the notches in the material. (2) Whether the linear elastic fracture mechanics (LEFM) or size effect law (SEL) were correctly applied. (3) Can the scratch test be regarded as a stable fracture state. New controversies [17, 18] followed, even though Akono *et al*. [19, 20] modified their models and limited their theory to a more specific condition. Both sides presented experimental results to support their position at least in some specific conditions. Although the debate is still unresolved, these studies have provided useful information for developing more advanced scratch test methods. Blackman *et al*. [21] used a specially designed blade, which can be applied along the crack direction to satisfy Ulm's assumption, and developed the concept of steady-state cutting of polymers with a sharp tool to evaluate the fracture property. In this paper, only one important assumption is used, that the crack direction is along the direction of the notches, as demonstrated in the experiment of Akono *et al*. [19]. A rectangular blade is used to reduce the frictional force and resolve other issues. Currently, the problem is unsolved for lack of stress–strain field information around the crack tip for the material with surface modification layer.

To investigate the fracture properties of surface modification layer with residual stress, the bi-layer beam model is a promising solution that allows one to calculate the energy release rate analytically without the detailed information of the stress-strain field near the crack tip. Suo and Hutchinson [22] developed the bi-layer model to study the interface crack between two elastic layers. In the bi-layer model, a semi-infinite crack is located at the interface of a bonded infinite long beams. As the crack propagates, the model remains similar to itself. So the stress-strain filed around the crack tip is always similar to that before the crack propagates. Moreover, the stress-strain fields far from the crack tip always tend to be homogeneous, so the energy release rate of the system can be easily calculated. Zhang *et al*. [23, 24] have used a similar pre-cracked semi-infinite parallel capacitor model to study the in-plane crack and interface crack problems under both electric and mechanical loadings. Zhao *et al*. [25, 26] have extended the bi-layer beam model to interfacial cracks of piezoelectric materials. Goutianos and Sorensen [27] have used a similar model under the framework of an elastic-plastic material and calculated the J-integral to measure cohesive laws under large-scale yielding.

In this paper, a modified bi-layer beam model is used to study the fracture scaling relations for scratch tests on brittle materials possessing a surface modification layer. The fracture-dominated problems are studied from the viewpoint of energy balance. In this model, the graded distribution of the elastic modulus, energy release rate and residual stress are considered in the modification layer. A nonlinear analytical solution is derived in Section 2, a well-developed finite element analysis method is used to model the surface modification layer in Section 3, the results and discussions are given in Section 4, and the conclusions are drawn in Section 5.

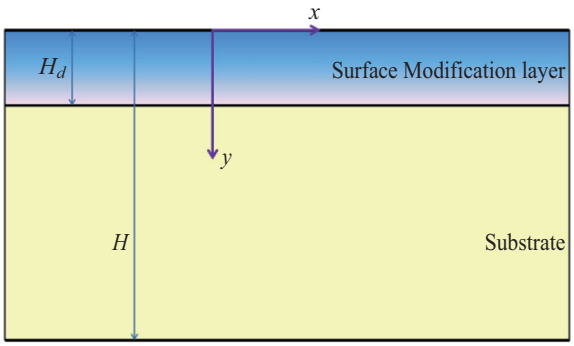


Fig. 1 Schematic plot of a substrate covered by a modification layer.

2. THEORETICAL FOUNDATION

Figure 1 is a schematic plot of a substrate covered by a modification layer. The coordinate system is set up with the x-axis along the surface and the y-axis pointing into the material. The Young's modulus is continuously changing in the modification layer and decreases or increases relative to that of the substrate. The Young's modulus E can be written in an exponential form [28] as

$$E=\begin{cases}E_0\exp\left(\alpha\left(1-y/H_d\right)\right), & y\le H_d,\\ E_0, & H_d<y<H,\end{cases} \tag{1}$$

where E_0 is the Young's modulus of the substrate, α is the decay coefficient of Young's modulus, H_d is the thickness of the surface modification layer, and H is the total thickness of the material.

Yang *et al*. [29] studied the residual stress profile induced by machining, and described the residual stress as an exponentially damped cosine function:

$$\sigma_r(x)=\sigma_{r0}\exp\left(\xi w_d y/\sqrt{1-\xi^2}\right)\cos\left(\pi y/H_d+\varphi\right), \tag{2}$$

where ξ is the damping coefficient, w_d is the damped frequency, φ is the phase angle, and σ_{r0} is the amplitude of the residual stress.

The fracture toughness of graded material can be expressed as an exponential form [30]. So the critical energy release rate G_c is assumed as

$$G_c=\begin{cases}G_0\exp\left(\eta\left(1-y/H_d\right)\right), & y\le H_d,\\ G_0, & H_d<y\le H,\end{cases} \tag{3}$$

where η is the decay coefficient of the energy release rate and G_0 is the critical energy release rate of the substrate.

Previous studies have shown that the Poisson ratio has little effect on functionally graded materials [30]. Thus, we take the Poisson ratio to be $\nu=0.3$.

For convenience, the parameters in Eqs. (1)-(3) are normalized by the substrate parameters. Only the case with a damping coefficient and phase angle equal to zero is considered in the present work and the residual stress in the substrate is ignored (the residual stress induced by machining is mianly located at the surface and decayed dramatically in the substrate). Then,

https://doi.org/10.1017/jmech.2018.36 Published online by Cambridge University Press

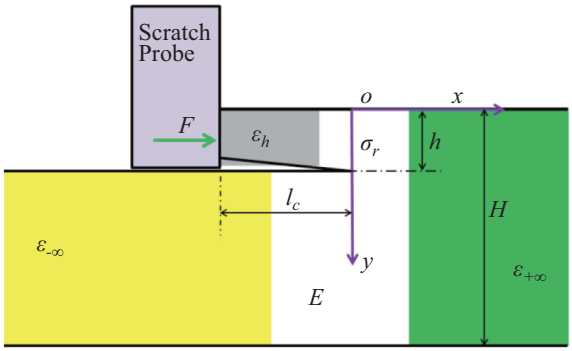


Fig. 2 Schematic of the modified bi-layer beam model.

$$\tilde{E}=\begin{cases}\exp\left(\alpha\left(1-\tilde{y}\right)\right), & 0<\tilde{y}\le 1,\\ 1, & 1<\tilde{y}\le \tilde{H},\end{cases} \tag{4}$$

$$\tilde{\sigma}_r=\begin{cases}\tilde{\sigma}_{r0}\cos\left(\pi\tilde{y}\right), & 0<\tilde{y}\le 1,\\ 0, & 1<\tilde{y}\le \tilde{H},\end{cases} \tag{5}$$

$$\tilde{G}_c=\begin{cases}\tilde{G}_0\exp\left(\eta\left(1-\tilde{y}\right)\right), & 0<\tilde{y}\le 1,\\ \tilde{G}_0, & 1<\tilde{y}\le \tilde{H},\end{cases} \tag{6}$$

where $\tilde{y}=y/H_d$, $\tilde{H}=H/H_d$, $\tilde{\sigma}_{r0}=\sigma_{r0}/E_0$, $\tilde{G}_0=G_0/E_0H_d$.

Figure 2 shows a schematic plot of the modified bi-layer beam model. Following the work of Ulm *et al.* [13, 14], a 2D crack problem is considered here. In Fig. 2, there is a crack at $y = h$, where the length of the crack l_c is assumed to be sufficiently large so that the strain in the cracked beam is nearly constant far from the crack tip. The stress–strain field is very important in fracture mechanics, and can be used to evaluate the stress intensity factor, the J-integral, and the energy release rate. In the bi-layer beam model (Fig. 2), the crack is assumed to be sufficiently long, and a scratch force F is applied to the scratch probe that causes the crack to propagate. When the crack propagates, the stress–strain field appears to move forward with the crack tip. The energy release rate can be obtained by comparing the differences in the elastic strain energies far ahead of the crack tip with those behind it. The strain fields far from the crack tip tend to be homogeneous in the x-direction, and they are used to calculate the energy release rate in the bi-layer beam model. The strain field far from the crack tip can be divided into three categories: the elastic strain far ahead of the crack tip ($\varepsilon_{+\infty}$, green areas in Fig. 2); the elastic strain far behind the crack tip below the crack ($\varepsilon_{-\infty}$, yellow area in Fig. 2) and above the crack (ε_h, gray area in Fig. 2).

The normalized scratch force and indentation depth are given by

$$\tilde{F}=F/E_0H_d, \tag{7a}$$

$$\tilde{h}=h/H_d. \tag{7b}$$

Note that the model considered in this paper is a 2D problem. Hence, the dimension of the concentrated force is the same as the dimension of E_0H_d.

The bi-layer beam model is a statically indeterminate problem; therefore, to solve the problem, an additional auxiliary equation is needed. We assume that the compressive displacement of the beam ahead of the crack tip is δ. Then, the strain far behind the crack tip and below the crack ($\varepsilon_{-\infty}$) and that far ahead of the crack tip ($\varepsilon_{+\infty}$) can be calculated using

$$\varepsilon_{-\infty}=\delta/L_{-\infty}, \tag{8a}$$

$$\varepsilon_{+\infty}=-\delta/L_{+\infty}, \tag{8b}$$

where $L_{-\infty}$ and $L_{+\infty}$ are the length of the beam behind and ahead of the crack tip, respectively. When the length of the bi-layer beam is assumed to be sufficiently long so that $L_{-\infty}= L_{+\infty}$, we have the auxiliary equation

$$\varepsilon_{-\infty}=-\varepsilon_{+\infty}. \tag{8c}$$

The constitutive relation gives

$$\tilde{\sigma}=\varepsilon\tilde{E}/\kappa+\tilde{\sigma}_r, \tag{9}$$

where $\kappa = 1$ for the plane stress state and $\kappa = 1 - \nu^2$ for the plane strain state.

The strain energy density is

$$\tilde{\psi}_i=\kappa\tilde{\sigma}^2/2\tilde{E}. \tag{10}$$

The force balance in the x-direction gives

$$\int_0^{\tilde{H}}\tilde{\sigma}_{+\infty}d\tilde{y}-\int_0^{\tilde{h}}\tilde{\sigma}_h d\tilde{y}-\int_{\tilde{h}}^{\tilde{H}}\tilde{\sigma}_{-\infty}d\tilde{y}=0, \tag{11}$$

where $\tilde{\sigma}_{+\infty}$, $\tilde{\sigma}_{-\infty}$ and $\tilde{\sigma}_h$ are the normalized stress far ahead of the crack tip, far behind the crack tip and above the crack, and that below the crack, respectively.

The stress far behind the crack tip and above the crack satisfies the relation

$$\int_0^{\tilde{h}}\tilde{\sigma}_h d\tilde{y}=-\tilde{F}. \tag{12}$$

Solving Eqs. (8c), (9), (11) and (12) yields

$$\varepsilon_{-\infty}=-\varepsilon_{+\infty}=\begin{cases}\dfrac{\kappa\alpha(\tilde{F}+\tilde{\sigma}_{r0}\sin(\pi\tilde{h})/\pi)}{2\alpha(\tilde{H}-1)+\exp(\alpha(1-\tilde{h}))+\exp(\alpha)-2}, & 0<\tilde{h}\le 1,\\ \dfrac{\kappa\alpha\tilde{F}}{\alpha(2\tilde{H}-\tilde{h}-1)+\exp(\alpha)-1}, & 1<\tilde{h}\le\tilde{H}.\end{cases} \tag{13}$$

Solving Eqs. (9) and (12), we obtain

https://doi.org/10.1017/jmech.2018.36 Published online by Cambridge University Press

Table 1 Comparison of the fracture toughness obtained from different methods in the homogeneous case.

NO.	1	2	3	4	5	6
K_c ($MPa\sqrt{m}$, Bi-layer beam model)	0.093	0.111	0.146	0.133	0.142	0.140
K_c ($MPa\sqrt{m}$, 3-point bending tests)	0.146	0.146	0.146	0.146	0.146	0.146
Error	36.1%	24.2%	0.1%	9%	3%	3.8%

$$\varepsilon_h = \begin{cases} -\dfrac{\alpha\kappa(\tilde{F}+\tilde{\sigma}_{r0}\sin(\pi\tilde{h})/\pi)}{\exp(\alpha)-\exp(\alpha(1-\tilde{h}))}, & 0<\tilde{h}\le 1, \\ -\dfrac{\alpha\kappa\tilde{F}}{\exp(\alpha)-1-\alpha(1-\tilde{h})}, & 1<\tilde{h}\le\tilde{H}. \end{cases} \tag{14}$$

The energy release rate can be calculated by

$$\tilde{G} = -\tilde{F}\varepsilon_h + \int_0^{\tilde{H}} \tilde{\psi}_{+\infty} d\tilde{y} - \int_0^{\tilde{h}} \tilde{\psi}_h d\tilde{y} - \int_{\tilde{h}}^{\tilde{H}} \tilde{\psi}_{-\infty} d\tilde{y}. \tag{15}$$

Substituting Eqs. (12), (13) and (14) into Eq. (15) gives

$$\tilde{G} = \begin{cases} -\tilde{F}\varepsilon_h + (\exp(\alpha)-\exp(\alpha(1-\tilde{h})))(\varepsilon_{-\infty}^2-\varepsilon_h^2)/2\kappa\alpha + \tilde{\sigma}_{r0}\sin(\pi\tilde{h})(\varepsilon_{-\infty}-\varepsilon_h)/2\kappa\alpha, & 0<\tilde{h}\le 1, \\ -\tilde{F}\varepsilon_h + (\exp(\alpha)+\alpha(\tilde{h}-1)-1)(\varepsilon_{-\infty}^2-\varepsilon_h^2)/2\kappa\alpha, & 1<\tilde{h}\le\tilde{H}. \end{cases} \tag{16}$$

It should be noted that Eqs. (13)-(16) could be reduced to the homogeneous case as Eqs. (17)-(19) if the elastic decay coefficient $\alpha = 0$.

$$\varepsilon_{-\infty} = -\varepsilon_{+\infty} = \begin{cases} \kappa(\tilde{F}+\tilde{\sigma}_{r0}\sin(\pi\tilde{h})/\pi)/(2\tilde{H}-\tilde{h}), & 0<\tilde{h}\le 1, \\ \kappa\tilde{F}/(2\tilde{H}-\tilde{h}), & 1<\tilde{h}\le\tilde{H}, \end{cases} \tag{17}$$

$$\varepsilon_h = \begin{cases} -\kappa(\tilde{F}+\tilde{\sigma}_{r0}\sin(\pi\tilde{h})/\pi)/\tilde{h}, & 0<\tilde{h}\le 1, \\ -\kappa\tilde{F}/\tilde{h}, & 1<\tilde{h}\le\tilde{H}, \end{cases} \tag{18}$$

$$G = \begin{cases} -\tilde{F}\varepsilon_h + (\varepsilon_{-\infty}^2-\varepsilon_h^2)\tilde{h}/2\kappa - \tilde{\sigma}_{r0}\sin(\pi\tilde{h})(\varepsilon_{-\infty}-\varepsilon_h)/\pi, & 0<\tilde{h}\le 1, \\ -\tilde{F}\varepsilon_h + (\varepsilon_{-\infty}^2-\varepsilon_h^2)\tilde{h}/2\kappa, & 1<\tilde{h}\le\tilde{H}. \end{cases} \tag{19}$$

Akono *et al*. showed the experimental results of scratch tests for paraffin wax [13]. When the w/d is big enough, the scratch tests could be viewed as a plane strain condition. We pick 6 points from Fig. 2 in reference [13], calculate the critical energy release rate G_c of paraffin wax using the bi-layer beam model. Then obtained the fracture toughness using a widely accepted equation $K_c = \sqrt{EG_c/\kappa}$. The calculated fracture toughness is compared with the Akono's experimental results from 3-point bending tests on notched specimen, as shown in Table 1. The average error between experimental analytical results is 12.7%, showing our analytical results is acceptable.

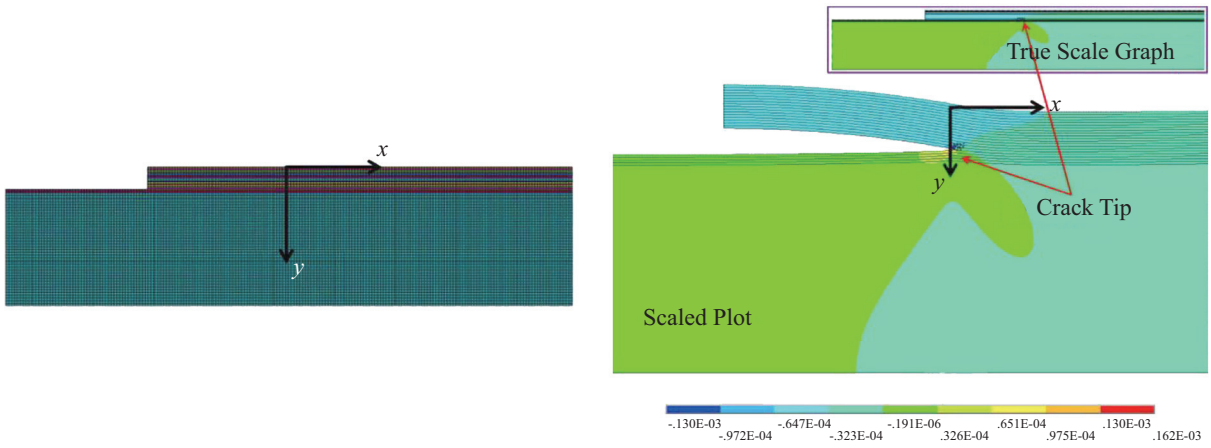
3. FINITE ELEMENT ANALYSIS

3.1 Finite Element Model

The FEM has been a widely accepted way to investigate mechanical fracture problems in graded materials. Simha *et al*. [31] have used FEM to simulate the fracture property in graded material. Recently, Shang *et al*. [32] used FEM to study the crack tip driving force of graded material.

Figure 3(a) shows the finite element mesh used for the modified bi-layer beam model generated directly by the ANSYS Parametric Design Language using a PLANE182 element. The length of the model L was set as 200, while the length of the crack $l_c = L/4$. In the numerical simulation, the thickness of the bi-layer beam H was changeable, varying from 2 to 10; the indentation depth varied between 0.2 to 2. A square element with a maximum element size of 0.1 was used in the substrate, while in the surface modification layer the element size was 0.02 to simulate the gradation of the material and the residual stress. The numerical convergence analysis was conducted for each condition. All the FEA results in the present paper are numerically convergent.

https://doi.org/10.1017/jmech.2018.36 Published online by Cambridge University Press



(a) (b)

Fig. 3 (a) Finite element meshes and (b) distribution of the x-component elastic strain in the bi-layer beam.

Table 2 Comparison between the theoretical normalized energy release rate and the numerical J-integral.

		Theoretical results	J_Path_1	J_Path_2	J_Path_3
Homogeneous No residual stress	Value	5.7305×10^{-9}	5.9256×10^{-9}	5.6331×10^{-9}	5.6245×10^{-9}
	Error	----	3.40%	1.70%	1.85%
Graded surface No residual stress	Value	8.5418×10^{-9}	8.5218×10^{-9}	8.5209×10^{-9}	8.5554×10^{-9}
	Error	----	0.23%	0.24%	0.16%
Graded surface residual stress	Value	1.2264×10^{-8}	1.2003×10^{-8}	1.2016×10^{-8}	1.2066×10^{-8}
	Error	----	2.13%	2.02%	1.61%

The color of the element in Fig. 3(a) represents the material number, where each material number was assigned a unique material property according to its position. The normalized Young's modulus of the substrate was 1, the Poisson ratio was 0.3, and the Young's modulus of the surface modification layer was calculated according to Eq. (4) with the elastic decay coefficient α varying from 0.2 to 5. The residual stress was also assigned to each material layer according to its location, where the normalized amplitude of the residual stress $\tilde{\sigma}_{r0}$ varied from -10^{-4} to 10^{-4}, and the residual stress of the surface modification layer was calculated according to Eq. (5). By assigning the appropriate material parameters to the elements according to their location, a gradation of the surface modification layer was simulated. Here, the gradation of the surface layer is modeled using many sub-layers where each sub-layer is assigned different materials. In the calculation, 50 sub-layers were used. The freedoms in the y-direction at the bottom of the beam were fixed, and the surfaces at the left side of the lower beam and the right side of the beam were supported and were able to slide. Finally, a homogeneously distributed force was applied to the left side of the upper layer beam.

3.2 FEM Results

The elastic strain in the areas far from the crack tip is uniform (Fig. 3(b)), which is the basis of the bi-layer beam model. It should be noted that the scaled plot (which is automatically calculated by the ANSYS software to show the details of the crack tip) doesn't reflect the real deformation. The true scaled plot is given in the top right corner in Fig. 3(b), which shows that the bending deformation is nearly invisible. We have proved both numerically and theoretically that the effect of bending is relatively small in the bi-layer beam model. The details are included in the Appendix. This FEM result demonstrates that it is reasonable to use the modified bi-layer beam model to simulate the scratch test on the surface modification layer. The numerical convergence analysis is conducted by using smaller element size.

Table 2 shows the theoretical normalized energy release rate and numerically calculated J-integrals using different integration paths with $\kappa = 0.91$, normalized residual stress $\tilde{\sigma}_{r0} = 10^{-4}$, normalized substrate thickness $\tilde{H} = 5$, normalized scratch force $\tilde{F} = 10^{-4}$, and elastic decay coefficients $e^{\alpha} = 0.2$. Path 1 starts from the point (−40, 0.8), and in turn passes the points (−40, 5), (90, 5) and (90, 0), and then extends to the upper crack face at (−40, 0.8), forming a counter-clockwise circuit. Similarly, Path 2 is (−20, 0.8)→(−20, 1.5)→(20, 1.5)→(20, 0.5)→(−20, 0.5)→(−20, 0.8), and Path 3 is (−5, 0.8)→(−5, 1)→(5, 1)→(5, 0.5)→(−5, 0.5)→(−5, 0.8). The numerically calculated J-integrals and the theoretical energy release are in good agreement. The

https://doi.org/10.1017/jmech.2018.36 Published online by Cambridge University Press

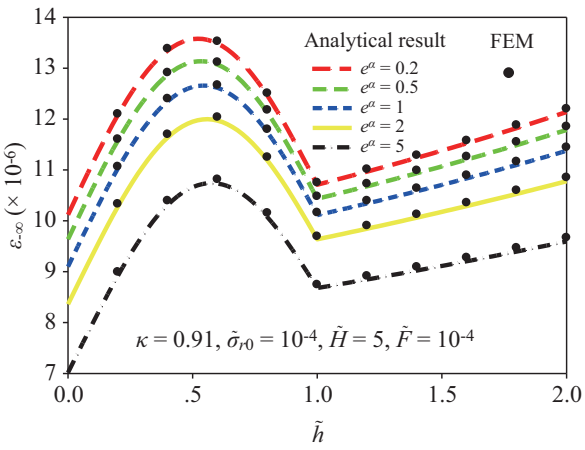


Fig. 4 The elastic strain far behind the crack tip below the crack versus the normalized indentation depth by the theoretical solution and FEM.

first group of data is for the homogeneous case without residual stress, while modification of the surface layer is considered in the second dataset. The good agreement between FEM results and theoretical results in Table 2 further proves that neglecting the effect of bending effect in the modified bi-layer model is appropriate.

4. RESULTS AND DISCUSSION

4.1 Strain Fields Far from the Crack Tip

The strain fields far from the crack tip are very important in the modified bi-layer beam model. In this initial step, the effects of the parameters on the strain fields are discussed.

Figure 4 shows the elastic strain far behind the crack tip below the crack $\varepsilon_{-\infty}$ versus the normalized indentation depth $\tilde{h}$ for the bi-layer beam model with κ = 0.91, normalized residual stress $\tilde{\sigma}_{r0} = 10^{-4}$, normalized substrate thickness $\tilde{H} = 5$, normalized scratch force $\tilde{F} = 10^{-4}$, and elastic decay coefficients e^α = 0.2, 0.5, 1, 2 and 5. The value of κ = 0.91 signifies a confined stress state with a Poisson's ratio ν = 0.3. The elastic decay coefficient α is used to describe the graded distribution of the Young's modulus within the modification layer. Here, e^α = 0.2 signifies that the Young's modulus of the surface is 0.2 times that of the substrate, where decreasing values of e^α denotes the increasing surface softness compared with the substrate. Specifically, $e^\alpha > 1$ means the surface is harder than the substrate, and $e^\alpha = 1$ means the layer is homogeneous. Each curve can be divided into two regions, where the first region resembles a downward parabola that initially increases, reaches its peak at $\tilde{h} \approx 0.5$, and then decreases until $\tilde{h}$ reaches 1. The second curve region starts at the ending point of the first region and increases almost linearly. It can be shown that when the surface modification layer is harder, the strain of the beam far behind the crack tip tends to be

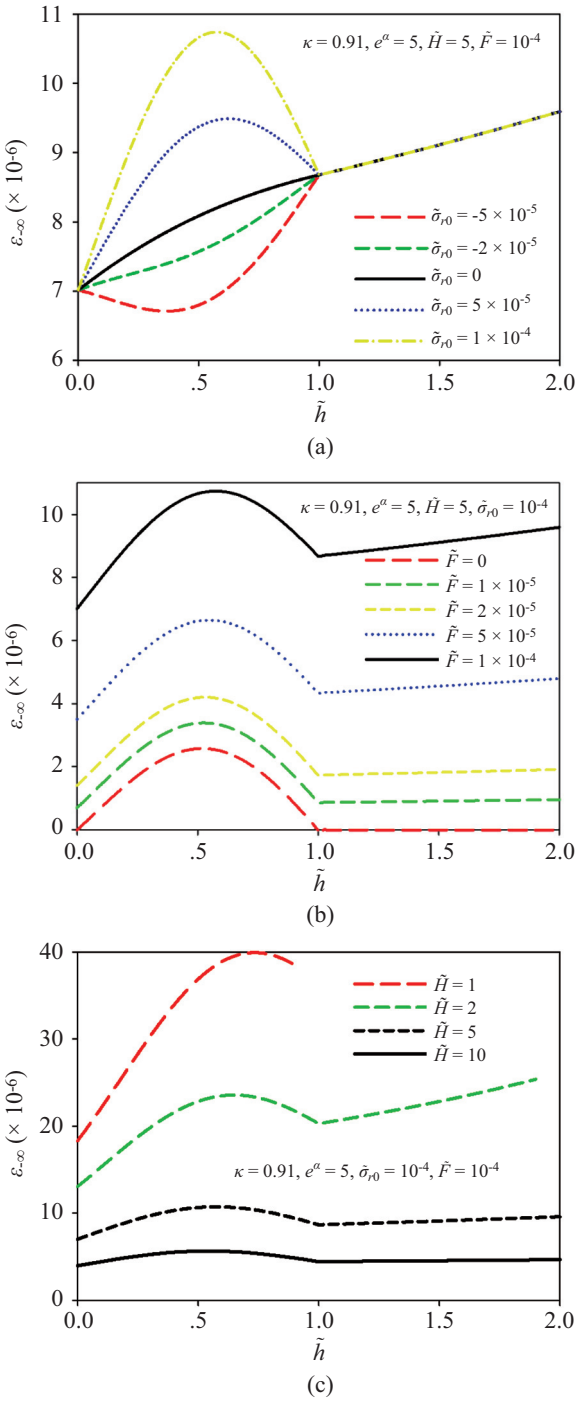


Fig. 5 The elastic strain far behind the crack tip below the crack versus the normalized indentation depth for (a) different normalized residual stress, (b) different normalized scratch force, and (c) different normalized total thickness.

smaller. These results obtained by the analytical solution are in good agreement with those obtained by the finite element solution.

Figure 5 plots the elastic strain far behind the crack tip below the crack $\varepsilon_{-\infty}$ versus the normalized indentation depth $\tilde{h}$ for different normalized amplitudes of residual stress $\tilde{\sigma}_{r0}$, normalized scratch forces $\tilde{F}$, and normalized total thicknesses $\tilde{H}$. Figure 5(a) shows the in-

https://doi.org/10.1017/jmech.2018.36 Published online by Cambridge University Press

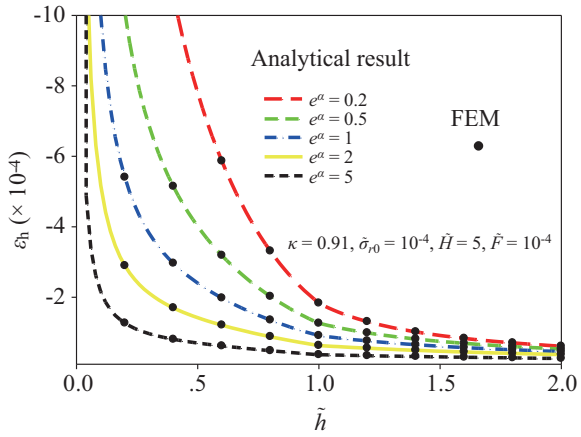


Fig. 6 The elastic strain far behind the crack tip above the crack versus the normalized indentation depth for different elastic decay coefficient.

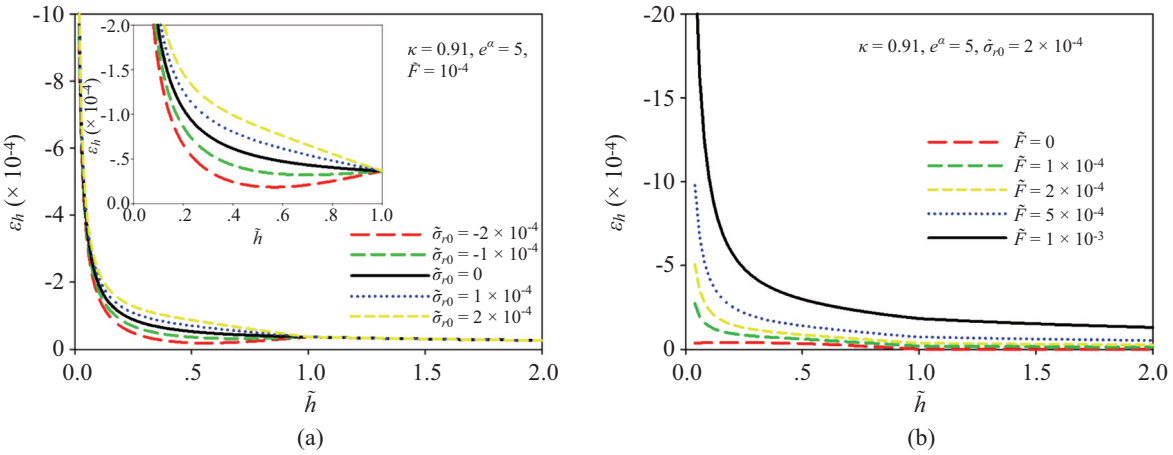


Fig. 7 The elastic strain far behind the crack tip above the crack versus the normalized indentation depth for (a) different normalized amplitude of residual stress, and (b) different normalized scratch force.

fluence of residual stress on $\varepsilon_{-\infty}$. When there is no residual stress, the inflection point disappears and the two different regions form a smooth curve. The residual stress affects the first portion of the curve only when the indentation depth is smaller than the thickness of surface modification layer. The shape of the curve in Fig. 5(a) is mainly affected by the residual stress, and $\varepsilon_{-\infty}$ increases with the normalized amplitude of residual stress. Fig. 5(b) shows $\varepsilon_{-\infty}$ versus $\tilde{h}$ for a varying normalized scratch force $\tilde{F}$. When the normalized scratch force is zero, the second region of the curve tends to zero, and the elastic strain increases dramatically with the normalized scratch force. Figure 5(c) plots $\varepsilon_{-\infty}$ versus $\tilde{h}$ for different $\tilde{H}$. It can be seen that as $\tilde{H}$ increases, the elastic strain is reduced. When $\tilde{H}$ decreases, the total stiffness of the bi-layer beam is reduced, which could lead to larger deformation.

Figure 6 shows the effect of the elastic decay coefficient e^{α} on the elastic strain far behind the crack tip and above the crack ε_h. A harder surface modification layer reduces the strain in the beam far from the crack tip. The finite element results are also provided in Fig. 6. It can be seen that there are in excellent agreement between FEM results with the theoretical results.

Figure 7 plots the elastic strain far behind the crack tip above the crack ε_h versus the normalized indentation depth $\tilde{h}$ with different normalized amplitude of residual stress, $\tilde{\sigma}_{r0}$, and normalized scratch force $\tilde{F}$. Figure 7(a) shows ε_h versus $\tilde{h}$ with a varying normalized residual stress $\tilde{\sigma}_{r0}$. The effect of normalized residual stress on ε_h is not significant. It is also noteworthy that no obvious transition can be found in the curve. The effect of the residual stress can be seen only when the indentation depth is smaller than the thickness of the surface modification layer (as shown in the inset of Fig. 7(a)), which is similar to that of the elastic strain far behind the crack tip under the crack. When the indentation depth increases, the strain tends to decrease until it reaches zero. Figure 7(b) shows ε_h versus $\tilde{h}$ for a varying normalized scratch force $\tilde{F}$. The elastic strain increases as the normalized scratch force increases, and the elastic strain tends to infinity when the normalized indentation depth approaches zero.

https://doi.org/10.1017/jmech.2018.36 Published online by Cambridge University Press

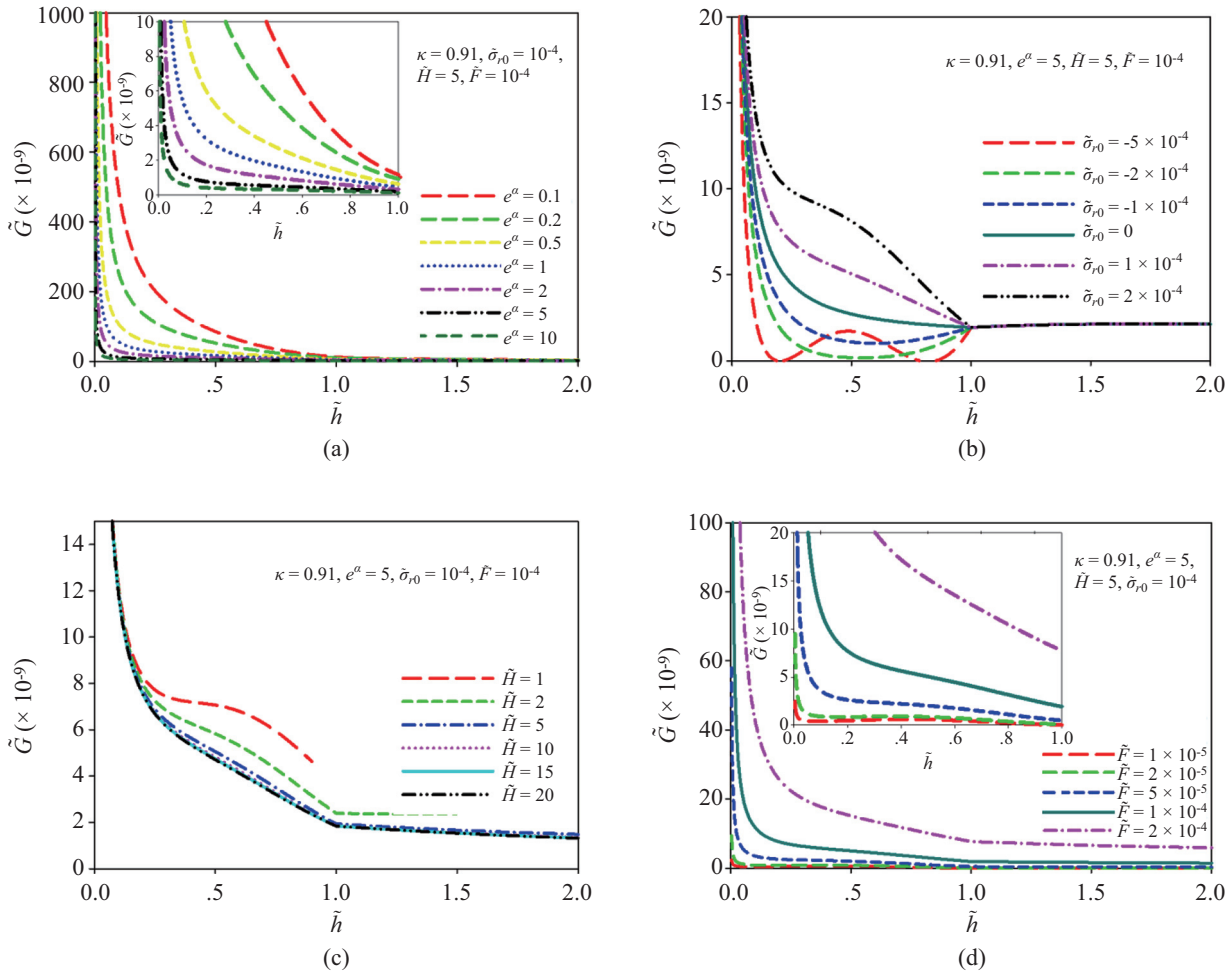


Fig. 8 Normalized energy release rate versus the normalized indentation depth for (a) different elastic decay coefficient, (b) different normalized amplitude of residual stress, (c) different normalized substrate thickness, and (d) different normalized scratch force.

4.2 Energy Release Rate

The energy release rate is a key parameter in fracture mechanics because when the energy release rate reaches a critical value, the crack starts to propagate.

Figure 8 shows the normalized energy release rate $\tilde{G}$ versus the normalized indentation depth $\tilde{h}$ for different elastic decay coefficient e^{α}, different normalized amplitude of residual stress $\tilde{\sigma}_{r0}$, different normalized substrate thickness $\tilde{H}$, and different normalized scratch force $\tilde{F}$.

Figure 8(a) shows the bi-layer beam model with κ = 0.91, normalized residual stress $\tilde{\sigma}_{r0} = 10^{-4}$, normalized substrate thickness $\tilde{H} = 5$, normalized scratch force $\tilde{F} = 10^{-4}$ and elastic decay coefficients e^{α} = 0.2, 0.2, 0.5, 1, 2, 5, and 10. We find that the energy release rate is affected by the elastic decay coefficient when the indentation depth is less than the thickness of the surface modification layer. It can also be obtained from Fig. 8(a) that $\tilde{G}$ decreases with the increase of e^{α}. The inset shows the same plot with the detailed information when the indentation depth is small.

Figure 8(b) shows the normalized energy release rate $\tilde{G}$ versus the normalized indentation depth $\tilde{h}$ for the bi-layer beam model using the values of κ = 0.91, e^{α} = 5, $\tilde{H} = 5$, $\tilde{F} = 10^{-4}$, and $\tilde{\sigma}_{r0} = -5\times10^{-4}$, -2×10^{-4}, -10^{-4}, 0, 10^{-4}, and 2×10^{-4}. The curves are separated into two regions; the residual stress has a significant influence in the first region but has almost no effect on the second region. The energy release rate shows an oscillation phenomenon when the amplitude of normalized residual stress gets down to -5×10^{-4}. To explain the mechanism of this phenomenon, we must examine the fracture process. The crack is a typical type-II mode crack where, in the absence of residual stress, the upper cantilever beam will be compressed and the lower cantilever beam below the crack will be stretched. However, when a residual compressive stress is applied, the lower cantilever beam will also be compressed. As the residual stress increases, a point is reached where the lower cantilever beam experiences the same compressed stress as does the upper beam. It seems that the structure are experienced a hydrostatic pressure, no crack propagation occurs at this point and the energy release rate is reduced to zero. As the residual compressive stress increases,

https://doi.org/10.1017/jmech.2018.36 Published online by Cambridge University Press

the lower cantilever beam suffers higher compressive stress, and it appears as if the lower cantilever beam is compressed and the upper beam is stretched. When the normalized amplitude of residual stress is -5×10^{-4}, which means the surface layer suffers a relatively high residual compressive stress. The crack is a type-II mode crack, the upper cantilever beam is always compressed, but the lower cantilever beam depends on the scratch force and the residual stress.The whole process can be separated into three phases. 1) When the normalized indentation depth is smaller than 0.2, as the indentation depth is relatively small, the residual stress cannot neutralize the scratch force applied by the indenter. The type-II mode crack behaves as if lower cantilever beam is stretched, and the upper cantilever beam is compressed. 2) As the indentation depth increases, the residual stress may completely neutralize the scratch force and cause the type-II mode crack behaves as if the upper cantilever beam is stretched. The energy release rate will reach its first valley at the transition point. 3) As the indentation depth further increases, the residual stress will be unable to neutralize the scratch force because the residual stress in the subsurface has the opposite value. One day the type-II mode crack behaves as if the upper cantilever beam is compressed again. At this point, the energy release rate will reach its second valley. Thus, the energy release rate shows an oscillation phenomenon when the amplitude of normalized residual stress gets down to -5×10^{-4}.

Figure 8(c) shows the normalized energy release rate $\tilde{G}$ versus the normalized indentation depth $\tilde{h}$ for the bi-layer beam model with κ = 0.91, e^{α} = 5, $\tilde{\sigma}_{r0} = 10^{-4}$, $\tilde{F} = 10^{-4}$, and $\tilde{H}$ =1, 2, 5, 10, 15, and 20. In Fig. 8(c), $\tilde{H} - 1$ is the normalized thickness of the substrate. It is seen that greater substrate thicknesses are associated with smaller energy release rates. Figure 8(d) shows the effect of $\tilde{F}$ on $\tilde{G}$. The graph shows that stronger normalized scratch forces are associated with larger energy release rates, and that the scratch force plays a dominant role in the energy release rate $\tilde{G}$. The inset shows the same plot with the detailed information when the indentation depth is small.

Figure 9 shows the normalized energy release rate $\tilde{G}$ versus the normalized indentation depth $\tilde{h}$ with varying normalized scratch forces $\tilde{F} = N \times 10^{-4}$, where N is affiliated with each curve. The solid black line in Fig. 9 denotes the critical energy release rate with $\tilde{G}_0 = 1.5 \times 10^{-7}$ and the critical energy release rate decay coefficient $e^{\eta} = 0.2$.

Taking the energy release rate as the failure criterion, the crack will propagate if

$$\tilde{G} \geq \tilde{G}_c, \tag{20}$$

where the normalized energy release rate $\tilde{G}$ (the driving force of the fracture) is determined by the structure geometry, the material properties and the scratch force. $\tilde{G}_c$ (the normalized critical energy release rate) denotes the material resistance against fracture, which is determined only by the material itself. At each indentation depth there is a cross-point of $\tilde{F}$ and $\tilde{G}_c$, which signifies that at each indentation depth there is a critical $\tilde{F}_c$, above which the crack will start propagating. When the energy release rate is smaller than that of $\tilde{G}_c$, however, the crack will not propagate. For a given $\tilde{h}$ and $\tilde{F}$, we can calculate the $\tilde{G}$ according to the formula obtained herein. Comparing $\tilde{G}$ with $\tilde{G}_c$, we can determine whether or not the crack will propagate.

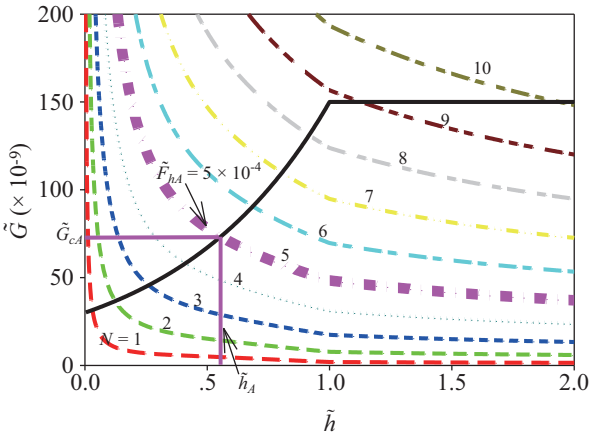


Fig. 9 Energy release rate versus the normalized indentation depth for κ = 0.91, e^{α} = 5, $\tilde{H} = 5$ and $\tilde{\sigma}_{r0} = 10^{-4}$ with different normalized scratch force $\tilde{F} = N \times 10^{-4}$, where N is affiliated with each curve. The black solid line denotes the critical energy release rate with $\tilde{G}_0 = 1.5 \times 10^{-7}$ and $e^{\eta} = 0.2$.

Assume that the critical energy release rate in the surface modification layer follows the form shown in Fig. 9. For a given normalized indentation depth $\tilde{h} = \tilde{h}_A$, there exists a critical normalized scratch force $\tilde{F}_{hA}$ driving the crack to propagate. Further, the critical normalized energy release rate at depth $\tilde{h}_A$ can be obtained from Fig. 9. Thus, we can determine the critical energy release rate at different depths according to the F–h curve (obtained from the scratch test) and the G–h curve (obtained from the present theoretical model). The critical energy release rate is unknown, but the scratch force versus the indentation depth can be obtained by experiment. Therefore, the inverse method can be used to determine the critical energy release rate and the fracture toughness. This is quite important for research involving surface modification layers, because the commonly used methods for measuring fracture properties are restricted to macro scale cases.

As surface modification layers are formed by many different mechanisms, the specific form of the material parameters and residual stresses may be changed for different mechanisms. However, it should be noted that changing the form of the function will not affect the

https://doi.org/10.1017/jmech.2018.36 Published online by Cambridge University Press

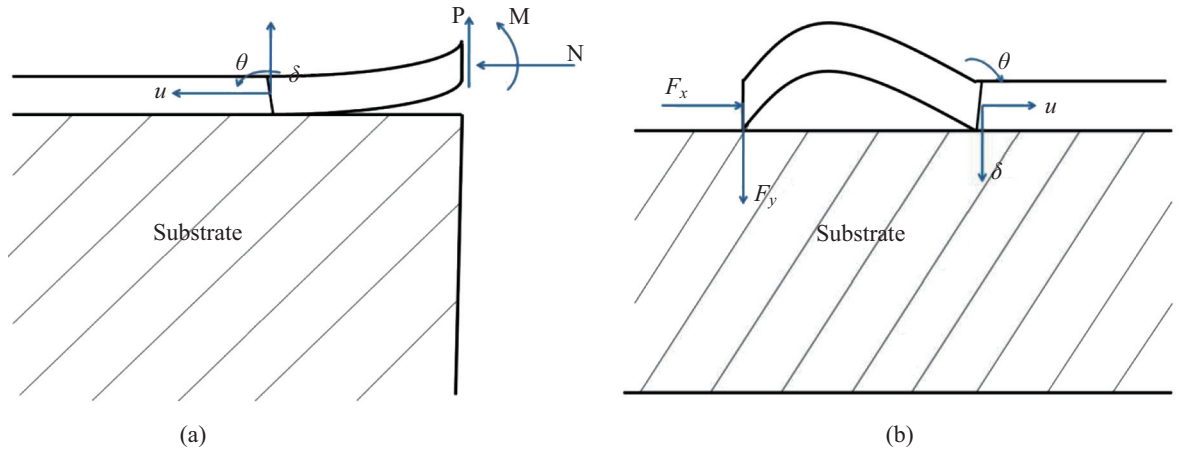


Fig. A1 A delaminated film attaches to a deformable substrate subjected to (a) bending moment M, axial load N and transverse shear load P, and (b) axial load F_x and transverse shear load F_y.

validity of our theoretical framework. The main purpose of this work is to develop a reliable method to determine the fracture parameters of materials with surface modification layers.

5. CONCLUSIONS

A modified bi-layer beam model is proposed to study the fracture scaling relations for scratch tests on brittle materials having a surface modification layer. The fracture dominated problems are studied from an energy point of view, where the Young's modulus and its decaying coefficient, the residual stress and the critical energy release rate are taken into consideration in the model. The following conclusions could be drawn.

1) Based on the great agreement between the finite element results and analytical results, the bi-layer beam model is proved to be suitable to assess the fracture properties of surface modification layer.
2) The scratch force and residual stress play an important role in the scale of the fractures in the scratch test. When the residual stress is well-controlled, the material resistance to crack propagation can be improved.
3) The Young's modulus and substrate thickness influence the elastic strain at all ranges, but only affect the energy release rate when the indentation depth is less than the thickness of the surface modification layer.
4) The present work, based on an inverse analysis method, is an efficient way to determine the fracture toughness of materials having a surface modification layer.

ACKNOWLEDGEMENTS

The work was supported by the National Natural Science Foundation of China (Nos. 11572289, 11272290 and 11702253). The authors declare that they have no conflict of interest.

APPENDIX

The effect of bending moment on scratch process of the homogenous materials.

Supposing the length of the cracked beam is long enough, we can use the beam theory to analyze the effect of bending moment on the scratch process of the homogenous materials. We take silicon wafer as a typical example and assume this silicon material to be mechanically isotropic with an average Young's modulus of 159 GPa and a Poisson ratio of 0.25. The effect of substrate deformation can be modeled by three coupled springs [33, 34]. As shown in Fig. A1(a), three generalized forces (force per unit width of the film), i.e., two forces, N and P, along the x-axis and the y-axis, respectively, and a moment (moment per unit width of the film), M, act on the three coupled springs and induce correspondingly three generalized displacements, u, δ and θ. A linear constitutive equation is applied

$$\begin{Bmatrix} u \\ \delta \\ \theta \end{Bmatrix} = \begin{bmatrix} S_{NN} & S_{NP} & S_{NM} \\ S_{PN} & S_{PP} & S_{PM} \\ S_{MN} & S_{MP} & S_{MM} \end{bmatrix} \begin{bmatrix} N \\ P \\ M \end{bmatrix}, \tag{A1}$$

where S_{ij} are the compliances and have the symmetry $S_{ij} = S_{ji}$. Fan *et al*. [34] gave the spring compliances for the silicon wafer with homogenous material when the support angle is 90°, as follows

$$\begin{aligned} &S_{MN} = S_{NM} = 1.61\times10^{-3}\,um/mN, \\ &S_{PM} = S_{MP} = 8.78\times10^{-3}\,um/mN, \\ &S_{PN} = S_{NP} = 9.81\times10^{-3}\,um^2/mN, \\ &S_{MM} = 1.43\times10^{-2}1/mN, \\ &S_{MN} = S_{NM} = 2.13\times10^{-2}\,um^2/mN, \\ &S_{PP} = 3.28\times10^{-2}\,um^2/mN, \end{aligned} \tag{A2}$$

https://doi.org/10.1017/jmech.2018.36 Published online by Cambridge University Press

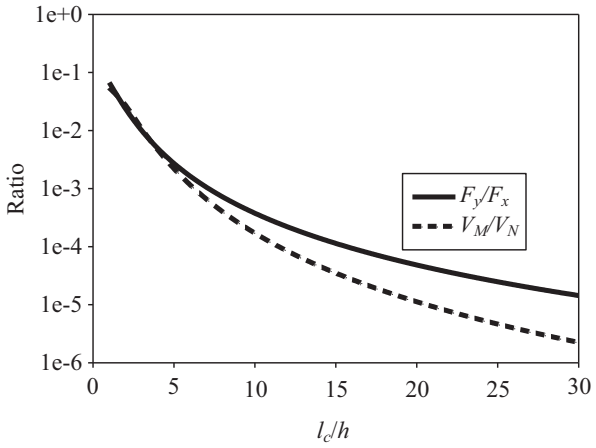


Fig. A2 The ratios of F_x/F_y and V_M/V_N vs l_c/h.

The indenter is assumed to attach to the indenter, so the end of the cantilever beam (contact area between the beam and indenter) has no transverse shear displacement and can rotate freely. The deformation of the substrate can be demonstrated by three generalized displacements, u, δ and θ, as shown in Fig. A1(b).

From force equilibrium, we have

$$M = -F_y l_c, \quad F_x = N, \quad F_y = -P. \tag{A3}$$

Assuming the beam is long enough and the deformation is relatively small, the beam theory can be used. From beam theory, we have

$$\theta = \frac{F_y l_c^2}{2EI}, \quad \delta = \frac{F_y l_c^3}{3EI}. \tag{A4}$$

where E = 159 GPa is the Young's modulus, l_c is the length of the crack, and $I = bh^3/12$ is the axial moment of inertia, in which b = 1 um and h = 1 um in the present example.

Combine Eqs. (A1-A4)

$$\frac{F_y l_c^3}{3EI} = S_{PN} F_x - S_{PP} F_y - S_{PM} l_c F_y. \tag{A5}$$

Then

$$F_y = \frac{S_{PN}}{l_c^3/3EI + S_{PP} + S_{PM} l_c} F_x. \tag{A6}$$

The strain energy caused by bending can be expressed by

$$V_M = \frac{M^2 l_c}{2EI} = \frac{F_y^2 l_c^3}{2EI}. \tag{A7}$$

The strain energy caused by axial loading is

$$V_N = \frac{1}{2}\frac{F_x^2 l_c}{Ebh}. \tag{A8}$$

where h is the thickness of delaminated layer. To investigate the influence of bending, we introduce different l_c/h and give the ratio of F_x/F_y and V_M/V_N, as shown in Fig. A2. The ratio of F_x/F_y and V_M/V_N decreases sharply as the increase of l_c/h. When the ratio of $l_c/h > 5$, the ratio of F_x/F_y and V_M/V_N are decreased to less than 0.01, which can be negligible, which means the energy caused by bending is relatively small compared with the effect of axial loading.

In the surface modification layer, the effect of substrate deformation is much more difficult to predict, so the beam theory is not applicable at the present stage. We can compare the theoretical result with the numerical result. As shown in Fig. 3(b), the scaled plot, which is automatically calculated by the ANSYS software to show the details of the crack tip, doesn't reflect the real deformation. The true scaled plot is plotted in the top right corner, which shows little bending deformation. What's more, the energy release rate calculated by the theoretical model (which assumes no bending occurs in the bi-layer beam model) has been compared to the J-integral calculated by FEM (where the delaminated beam can bend freely), the results in Table 2 show that there is only a relatively small difference. Above all, neglecting the bending effect in the bi-layer beam model is reasonable.

NOMENCLATURE

Acronyms:

FEM	Finite Element Method
SEL	Size Effect Law

Symbols:

$\tilde{\chi}$	the normalized value of χ, χ represents any variables below
α	elastic decay coefficient
$\varepsilon_{+\infty}$	elastic strain far in front of the crack tip
$\varepsilon_{-\infty}$	elastic strain far behind the crack tip and below the crack
ε_h	elastic strain far behind the crack tip and above the crack
η	decay coefficient of the energy release rate
κ	κ = 1 for plane stress state and κ = 1– ν^2 for plane strain state
ξ	damping coefficient of the residual stress
φ	phase angle of the residual stress
ν	Poisson ratio
$\tilde{\sigma}_{+\infty}$	elastic stress far in front of the crack tip
$\tilde{\sigma}_{-\infty}$	elastic stress far behind the crack tip and below the crack
$\tilde{\sigma}_h$	elastic stress far behind the crack tip and above the crack
$\Psi_{+\infty}$	strain density far ahead the crack tip
$\Psi_{-\infty}$	strain density far behind the crack tip below the crack
Ψ_h	normalized strain density far behind the crack tip above the crack

https://doi.org/10.1017/jmech.2018.36 Published online by Cambridge University Press

$\tilde{\sigma}_r$	residual stress
$\tilde{\sigma}_{r0}$	the amplitude of the residual stress
x, y	x and y coordinate
h	indentation depth
E	Young's modulus
E_0	Young's modulus of the substrate
F	scratch force in the tangential direction
F_{hA}	minimum scratch force when the indentation depth is h_A, and the critical energy release rate is G_{cA}
G	energy release rate
G_c	critical energy release rate
G_{cA}	maximum critical energy release rate when scratch force is F_{hA}, and indentation depth is h_A
G_0	critical energy release rate of the substrate
H	thickness of the bi-layer beam model
H_d	thickness of the surface modification layer
l_c	length of the crack
$L_{+\infty}$	length of the beam in front of the crack tip
$L_{-\infty}$	length of the beam behind the crack tip
S_{ij}	spring compliances for the coupled springs
u, δ, θ	generalized displacements in the coupled springs
M, N, P	generalized forces in the coupled springs
F_x, F_y	axial and transverse shear load in the bi-layer beam model
V_M	strain energy caused by bending
V_N	strain energy caused by axial loading

REFERENCES

1. Podgornika, B., Sedlaceka, M. and Cekadab, M., "Impact of Fracture Toughness on Surface Properties of PVD Coated Cold Work Tool Steel," *Surface & Coatings Technology*, **277**, pp. 144-150 (2015).
2. Ju, H. B. *et al*., "The Enhancement of Fracture Toughness and Tribological Properties of the Fitanium Nitride Films by Droping Yttrium," *Surface & Coatings Technology*, **321**, pp. 57-63 (2017).
3. Chen, L. H., Huang, K. C. and Chen, Y. C., "Acoustic Emission at Wedge Indentation Fracture in Quasi-Brittle Materials," *Journal of Mechanics*, **25**, pp. 213-223 (2009).
4. Huang, B., Zhao, M. H. and Zhang, T. Y., "Indentation Fracture and Indentation Delamination in ZnO Film/Si Substrate Systems," *Philosophical Magazine*, **84**, pp. 1233-1256 (2004).
5. Prasad, A., Dao, M. and Suresh. S., "Steady-State Frictional Sliding Contact on Surfaces of Plastically Graded Materials," *Acta Materialia*, **57**, pp. 511-524 (2009).
6. Zhang, F. Y., Duan, C. Z. and Wang, M. J., "Research Status of the Machined Surface Metamorphic Layer," *Machinery Design & Manufacture*, **10**, pp. 265-268 (2014).
7. Zhu, Z. Y. and Zhang, J. L., "The Study on Mechanical Property of the Metamorphic Layer after Electron Discharge Machining for Die Steels," *Materials for Mechanical Engineering*, **68**, pp. 48-52 (1988).
8. Ma, F. B. and Chen, S. F., "Study of Surface Modification Layer has Been Processed," *Coal Mine Machinery*, **34**, pp. 113-114 (2013).
9. Cao, H. Y., "Analysis and Calculation of EDM Mold Surface Deterioration Layer," *Mechanical Engineer*, **4**, pp. 58-59 (2010).
10. Lida, K. and Tosha, K., "Behavior of Surface Residual Stress Induced by Shot Peening (II)," *Advances in Surface Treatments*, **52**, pp. 139-144 (1987).
11. Gee, M. G., "Low Load Multiple Pass Scratch Testing for Ceramics and Hardmetals," *Wear*, **250**, pp. 264-281 (2001).
12. Jiang, H., Zhang, J. W., Yang, Z. R., Jiang, C. K. and Kang, G. Z., "Modeling of Competition between Shear Yielding and Crazing in Amorphous Polymers' Scratch," *International Journal of Solids and Structures*, **124**, pp. 215-228 (2017).
13. Akono, A. T., Reis, P. M. and Ulm, F. J., "Scratching as a Fracture Process: From Butter to Steel," *Physical Review Letters*, **106**, pp. 204302 (2011).
14. Akono, A. T. and Ulm, F. J., "Scratch Test Model for the Determination of Fracture Toughness," *Engineering Fracture Mechanics*, **78**, pp. 334-342 (2011).
15. Lin, J. S. and Zhou, Y. N., "Can Scratch Tests Give Fracture Toughness?" *Engineering Fracture Mechanics*, **109**, pp. 161-168 (2013).
16. Lin, J. S. and Zhou, Y. N., "Rebuttal: Shallow Wide Groove Scratch Tests Do Not Give Fracture Toughness," *Engineering Fracture Mechanics*, **133**, pp. 117-124 (2014).
17. Le, J. L. and Detournay, E., "Discussion on the "Fracture Mechanics Interpretation of the Scratch Test" by Akono *et al.*," *Engineering Fracture Mechanics*, **168**, pp. 46-50 (2016).
18. Zhou, Y. N., "Discussion on the Interpretation of Scratch Tests with Size Effect Law," *Engineering Fracture Mechanics*, **169**, pp. 178-183 (2017).
19. Akono, A. T. and Ulm, F. J., "An Improved Technique for Characterizing the Fracture Toughness via Scratch Test Experiments," *Wear*, **313**, pp. 117-124 (2014).
20. Akono, A. T. and Gregory, A. B., "Rebuttal: Shallow and Deep Scratch Tests as Powerful Alternatives to Assess the Fracture Properties of Quasi-Brittle Materials," *Engineering Fracture Mechanics*, **158**, pp. 23-38 (2016).
21. Blackman, B. R. K., Hoult, T., Patel, Y., Steininger, H. and Williams, J. G., "Steady-State Scratch Test-

https://doi.org/10.1017/jmech.2018.36 Published online by Cambridge University Press

ing of Polymers," *Polymer Testing*, **49,** pp. 38-45 (2016).

22. Suo, Z. G. and Hutchinson, J. W., "Interface Crack between Two Elastic Layers," *International Journal of Fracture*, **25**, pp. 1337-1353 (1989).
23. Zhang, T. Y. and Xie, T., "Effect of Electrostatic Tractions on the Fracture Behavior of a Dielectric Material under Mechanical and/or Electric Loading," *Science China: Technological Sciences*, **55**, pp. 2391-2403 (2012).
24. Xie, T., Fan, C. Y., Liu, H. T., Zhao, M. H. and Zhang, T. Y., "Effect of Electrostatic Trations on the Fracture Behavior of a Piezoelectric Material under Mechanical and/or Electric Loading," *Theoretical Applied Fracture Mechanics*, **69**, pp. 6-16 (2014).
25. Zhao, M. H., Liu, H. T., Fan, C. Y., Pan, E. and Zhang, T. Y., "A Nonlinear Bilayer Beam Model for an Interfacial Crack in Dielectric Bimaterials under Mechanical/Electrical Loading," *International Journal of Fracture*, **188**, pp. 47-58 (2014).
26. Zhao, M. H., Liu, H. T., Xu, G. T. and Fan, C. Y., "Effects of Electrostatic Tractions on the Interfacial Fracture Behavior of Two-Phase Piezoelectric Materials", *Engineering Fracture Mechanics*, **153**, pp. 289-301 (2016).
27. Goutianos, S. and Sorensen, B. F., "The Application of J Integral to Measure Cohesive Laws under Large-Scale Yielding," *Engineering Fracture Mechanics*, **155**, pp. 145-165 (2016).
28. Luo, Q. H., Li, C. Z., Luo, Y. Z. and Zhao, Z. Y., "Grinding Process Effect on Surface Modificative Layer Microstructure, Property and Fatigue Behavior of Carburized M50NiL Steel," *Acta Metallurgica Sinica*, **48**, pp. 194-198 (2012).
29. Yang, D., Liu, Z. Q., Ren, X. P. and Zhuang, P., "Hybrid Modeling with Finite Element and Statistical Methods for Residual Stress Prediction in Peripheral Milling of Titanium Alloy Ti-6Al-4V," *International Journal of Mechanical Science*, **108**, pp. 29-38 (2016).
30. Jin, Z. and Batra, R. C., "Some Basic Fracture Mechanics Concept in Functionally Graded Materials," *Journal of the Mechanics and Physics of Solids*, **44**, pp. 1221-1235 (1996).
31. Simha, N. K., Fischer, F. D., Kolednik, O. and Chen, C.R., "Inhomogeneity Effects on the Crack Driving Force in Elastic and Elastic-Plastic Materials," *Journal of Mechanics and Physics of Solids*, **51**, pp. 334-342 (2003).
32. Shang, Y. B., Shi, H. J., Wang, Z. X. and Zhang, G. D., "A Crack Tip Driving Force Model for Mode I Crack Propagation Along Linear Strength Gradient: Comparison with the Sharp Strength Gradient Case," *Acta Mechanica*, **227**, pp. 2683-2702 (2016).
33. Zhang, T. Y., Zhao, M. H. and Qian, C. F., "Effect of Substrate Deformation on the Microcantilever Beam-Bending Test," *Journal of Materials Research*, **15**, pp. 1868-1871 (2000).
34. Fan, C. Y., Zhao, M. H., Zhu. Y. J., Liu, H. T. and Zhang, T. Y., "Analysis of Micro/Nanobridge Test Based on Nonlocal Elasticity," *International Journal of Solids and Structures*, **49**, pp. 2168-2176 (2012).

(Manuscript received March 20, 2018, accepted for publication July 4, 2018.)

https://doi.org/10.1017/jmech.2018.36 Published online by Cambridge University Press